

CONVOLUTIONAL CODES ACTING AS EMI VIRTUAL SHIELDS IN CURRENT INJECTION SYSTEMS

F. Faghihi, H. Heydari, A. Falahati, and Y. Attar Easy

Center of Excellence for Power System Automation and Operation
Electrical Engineering Department
Iran University of Science and Technology
Tehran, Iran

Abstract—In order to design high current devices, there are many factors to be considered, such as the compatibility of these devices with internal and external propagation, as well as the generation of low- and high-frequency disturbances within electromagnetic environments.

This paper reports the simulation and measurement results of the electromagnetic interference (EMI) due to the fields inside and outside a Current Injection Transformer (CIT) and its control system during short circuit tests. This paper also pushes the state of the art by proposing a synthetic algorithm based on a channel coding technique for error free EMI shielding to increase the performance level of the CIT against the unpredictable events of the likelihood of transient states accompanying EMI which may result in the malfunctioning of the control system and data exchanges through the connectors.

1. INTRODUCTION

For an electrical utility you have the right to demand that every piece of power equipment installed on your system meets your exact specifications. The reliability and safety of your system depend on all the components performing as intended. As a manufacturer, the performance and conformance to industry standards of your product are of prime importance. Testing can assure that your product meets or exceeds performance standards. High currents of a current injection system (CIS) can propagate electromagnetic fields during tests and electromagnetic compatibility (EMC) considerations become an important aspect in the system [1]. Therefore, appropriate shields for mitigation of electromagnetic interference (EMI) must be designed [2]. For this purpose, studies on different shielding materials and

structures as classic methods have been carried out [3, 4]. Most simply, accurate performance of the control system is ensured by the construction of good shields for its packaging box while the radiated disturbance fields are present. Regarding all methods to mitigate EMI, the probability of undesired alteration to transmitted information of a control system can not be ignored. This weakness can be solved only by error correction methods [5, 6]. For error correction, different methods such as convolutional codes, turbo codes, etc., are available in the literature [7, 8] and can be modified for Current Injection Systems (CIS) as a secondary shielding process. The design of appropriate coding as secondary EMC protection depends on the software and hardware characteristics of the system.

Hence comes the need for advanced numerical techniques for correctly calculating bit error rate (BER) performance and the optimized code rate is identified regarding the system characteristics, which is the main motivation for initiating this paper.

2. FEM MATHEMATICAL ANALYSIS

The simulations are based on the edge element method and the magnetic vector potential method [9–11]. The former method constitutes the theoretical foundation of the low frequency EMF element.

The vector potential method is applicable for both 2-D and 3-D electromagnetic fields. Considering static and dynamic fields, and neglecting displacement currents (quasi-stationary limit), the following subset of Maxwell's equations apply:

$$\nabla \times \{H\} = \{J\} \quad (1)$$

$$\nabla \times \{E\} = - \left\{ \frac{\partial B}{\partial t} \right\} \quad (2)$$

$$\nabla \cdot \{B\} = 0 \quad (3)$$

The basic equation to be solved is in the form of:

$$[C] \{\dot{u}\} + [K]\{u\} = \{J_i\} \quad (4)$$

The terms of this equation are defined below; the edge field formulation matrices are obtained from these terms with the following boundary conditions.

Degree of freedom:

$$\{u\} = \left\{ \begin{array}{l} \{A_e\} \\ \{v_e\} \end{array} \right\} \quad (5)$$

where $\{A_e\}$ and $\{v_e\}$ are the magnetic vector potential and time integrated electric scalar potential, respectively.

Coefficient matrices:

$$[\bar{K}] = \begin{bmatrix} [K^{AA}] & [0] \\ [K^{vA}] & [0] \end{bmatrix} \quad (6)$$

$$[K^{AA}] = [K^L] + [K^N] + [K^G] \quad (7)$$

$$[K^L] = \int_{vol} (\nabla \times [N_A]^T)^T [v] (\nabla \times [N_A]^T - [N_A][\sigma] (\{v\} \times \nabla \times [N_A]^T)) d(vol) \quad (8)$$

$$[K^G] = \int_{vol} (\nabla \cdot [N_A]^T)^T [v] (\nabla \cdot [N_A]^T) d(vol) \quad (9)$$

$$[K^N] = 2 \int_{vol} \frac{dv_h}{d(|B|^2)} (\{B\}^T (\nabla \times [N_A]^T))^T (\{B\}^T (\nabla \times [N_A]^T)) d(vol) \quad (10)$$

$$[K^{vA}] = - \int (\nabla [N]^T)^T [\sigma] \{v\} \times \nabla \times [N_A]^T d(vol) \quad (11)$$

$$[C] = \begin{bmatrix} [C^{AA}] & [C^{Av}] \\ [C^{Av}]^T & [C^{vv}] \end{bmatrix} \quad (12)$$

$$[C^{AA}] = \int_{vol} [N_A][\sigma][N_A]^T d(vol) \quad (13)$$

$$[C^{Av}] = \int_{vol} [N_A][\sigma] \nabla \{N\}^T d(vol) \quad (14)$$

$$[C^{vv}] = \int_{vol} (\nabla \{N\}^T)^T [\sigma] \nabla \{N\}^T d(vol) \quad (15)$$

- Applied loads:

$$\{J_i\} = \begin{Bmatrix} \{J^A\} \\ \{I^t\} \end{Bmatrix} \quad (16)$$

$$\{J^A\} = \{J^S\} + \{J^{pm}\} \quad (17)$$

$$\{J^S\} = \int_{vol} \{J_s\} [N_A]^T d(vol) \quad (18)$$

$$\{J^{pm}\} = \int_{vol} (\nabla \times [N_A]^T)^T \{Hc\} d(vol) \quad (19)$$

$$\{I^t\} = \int_{vol} \{J_t\} [N_A]^T d(vol) \quad (20)$$

where $[N_A]$, $\{N\}$, $\{J_s\}$, $\{J_t\}$, vol , $\{H_c\}$, v_o , $[v]$, $\frac{dv_h}{d(|B|)^2}$, $[\sigma]$, and $\{v\}$ are matrix of element shape function for $\{A\}$, vector of element shape function for $\{V\}$, source current density vector, total current density vector, volume of the element, coercive force vector, reluctivity of free space, partially orthotropic reluctivity matrix, derivative of reluctivity with respect to the magnitude of magnetic field squared, orthotropic conductivity, and velocity vector respectively.

The magnetic field density is the first derived result. It is defined as the curl of the magnetic vector potential. This evaluation is performed at the integration points using the element shape function:

$$\{B\} = \nabla \times [N_A]^T \{A_e\}. \quad (21)$$

where, $\{B\}$ and $\{A_e\}$ are the magnetic field density and nodal magnetic vector potential respectively.

3. EMC ISSUES

Due to the high current from the output terminals of the CIT, the EMC issues for the sensitive part of the system (control circuits) are very crucial. Fig. 1 shows 3D modeling of the field intensity propagation of a 25 KA busbar in an air environment with infinite boundary conditions.

The control circuit of the CIS consists of a timer, pulse generator for triggering switching elements with logic gates, a microprocessor, and wires and appropriate connections. EMI with this circuitry can cause some ambiguities in control signals [12, 13]. It is evident in Fig. 2, that the unwanted noise due to radiation fields can be combined with the transmitted signals. As a result, the data 0001 could be converted into 1111 [14]. The radiation fields can also induce a voltage on the ground point of the control circuit, giving rise to changes in the ground voltage. Indeed, suitable shielding is one of the crucial factors against EMI in the control unit of the CIS.

Figure 3 illustrates the flux density distribution in the enclosure of the CIS which verifies the importance of sensitive element shielding.

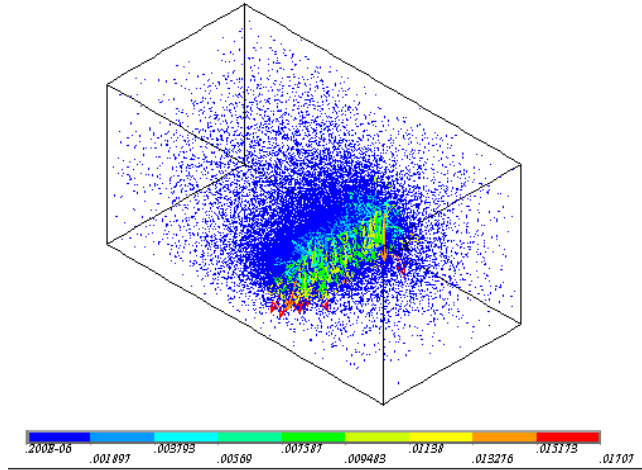


Figure 1. 3D modeling of the field intensity propagation of a 25 KA busbar in an air environment with infinite boundary conditions.

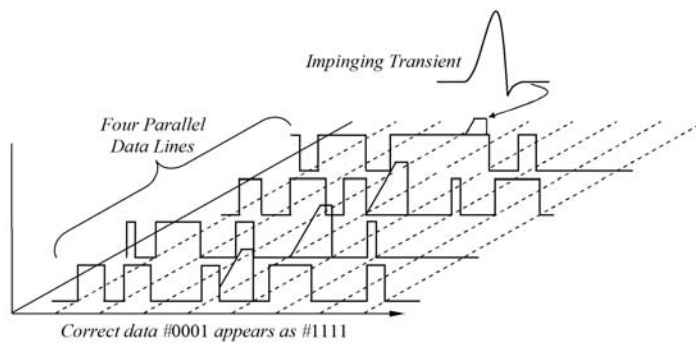


Figure 2. Control data signaling in combination with unwanted transient signals [14].

3.1. Design of Shielding Enclosure

The major items in the design of a shielded room are material, thickness, and the structure of the shields. Multi-layer shielding is a method of designing a shield structure. In this method, the major parameters are the number of layers, that is, the thickness of each layer and the distances between layers.

Iron has a high relative permeability so that for frequencies below 100 Hz and for thicknesses less than 5 mm, its “shielding effectiveness”

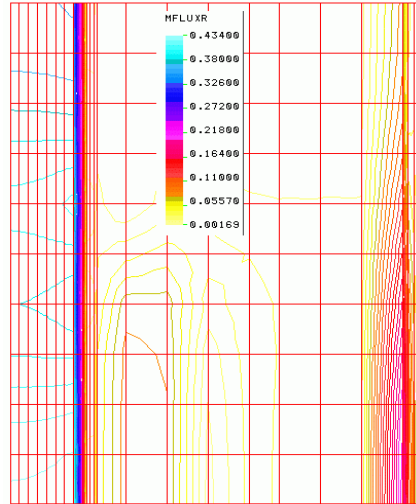


Figure 3. The distribution of flux density in the CIS enclosure.

(SE) is suitable [3]. A 4 mm thickness of iron is an acceptable shield in a 25 kA environment and can result in 68 dB SE [15].

Generally, SE is used as a “figure of merit” for gauging the attenuation of an electromagnetic field through a shielding barrier material. The concept of SE is based on wave theory and can be computationally complex and requires the understanding of the associated physics [4], so, the numerical analysis were carried out by experimental measurements employing a Gaussmeter.

In this study, to achieve the best shielding in six layers at 50 Hz, a sheet of iron having 6 mm thickness was used in the field simulations. The exterior surface of the last layer at a 556 mm distance from the source was considered in all cases, through the following steps

- a) A single layer shield with 6 mm thickness at 550 mm away from the source.
- b) A two layer shield with 3 mm thickness and with 5 cm gap in between.
- c) A three layer shield with 2 mm thickness with 2.5 cm gap in between.
- d) A four layer shield with 1.5 mm thickness and with a 2.2 cm gap in between.
- e) A five layer shield with 1.2 mm thickness and with a 1.25 cm gap in between (Fig. 4).
- f) A six layer shield with 1 mm thickness and with a 1 cm gap in between.

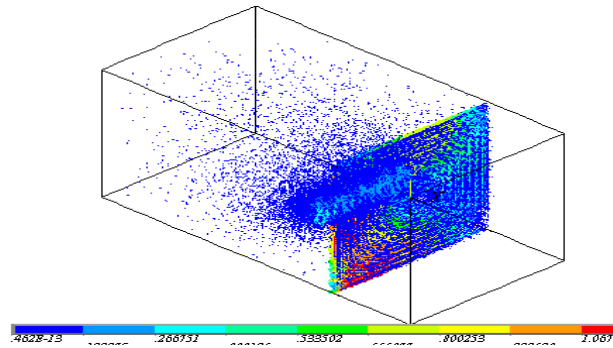


Figure 4. 3D modeling of the field intensity attenuation considering five layer iron shields.

Since the simulation result shown in Fig. 4 gives only a rough picture about the dispersed field, it is important to run controlled experiments to compare the relative effectiveness of the measurement results for evaluation of the material’s SE. Thus, based on the shielding effectiveness relationship: $SE = 20 \log \frac{B_{out}}{B_{in}}$ (dB), the input field (B_{in}) and the output field (B_{out}) are precisely measured using a Gaussmeter. Based on the average of the SE across the shield for the iron material for all of the above cases, the five layer shield is found to produce the best SE, as depicted in Fig. 5. It is shown that, by increasing the number of shielding layers, the SE is increased up to five layer shielding, giving a 70% improvement in SE with respect to one single layer with 6 mm thickness. Hence, in the multi-layer shielding technique, based on distance and thickness, the material SE is improved.

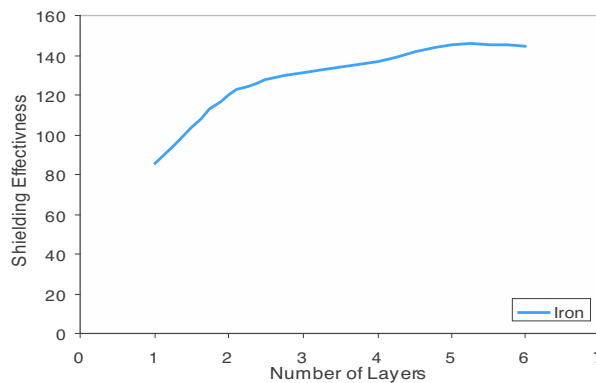


Figure 5. The SE (dB) of one to six layers iron with 6mm thickness.

4. APPLICATION OF CONVOLUTIONAL CODES OVER CIS CONTROL SYSTEM AS A VIRTUAL SHIELDING

Regardless of EMC appliances, there is undesired interference for special conditions, such as electromagnetic field penetration through the shielding barrier, transients causing inaccurate performance of the control circuits, or transmission signals passing through the wires. Hence, the design of the error free system by the employment of error correction codes can increase the reliability factor of the whole system from an EMC standards point of view which is termed "*Secondary Shielding*". Thus, an error correction code based on convolutional codes [5, 6] with minimum delay as a secondary shielding to achieve a suitable level of error free system design is desired. In the CIS enclosure, the data transmitted by the temperature sensor are very sensitive to EMI, so a set of encoders and decoders for implementation of convolutional codes is required. It will create more error free outputs with a good timing diagram.

While the embodiment of the proposed approach is described herein by way of a case study (CIS), those skilled in the art will appreciate that various modifications, alterations, and adaptations to the described system may be realized without departing from the spirit and scope of the work.

4.1. System Characteristics

Electrical equipment such as circuit breakers, protective relays, and meters are routinely tested to verify the proper operation of the current sensing elements.

To accomplish the proposed coding algorithm, a 25 kA, CIS which is considered here as a case study was, as mainly incorporating a 25 kA–125 kVA transformer delivering an output secondary current (25 kA), as closely as possible proportioned to the primary current at relative low voltages (1 to 5 Volts) [15, 16].

A microprocessor controlled tapchanger system is designed to suit the testing of different currents ranging from 0 to 25 kA, as shown in Fig. 6. This figure shows the circuit diagram of the current control system consisting of three main parts: A, B, and C. A tapchanger and discrete autotransformer (A) with 12 tap (each of which 35 V) output is initially setup.

For accurate operation, the output of the discrete autotransformer is connected to a continuous autotransformer (Variac) (B section) in series from which the Variac adds the voltage between 0–35 V to the output. The range of 0 to 35 V of the Variac is adjusted by the auxiliary

transformer (C section). Both autotransformers are controlled by a flexible programmable gate array (FPGA) chip.

Table 1. Design parameters of 25 kA CIT.

Rating	Capacity	125 kVA
	Voltage	400/5 V
	Current	312.5/25000A
	Frequency	50 Hz
Core	Material	30M5
	Max. Flux Density	1.6 T
	Pure Cross Section	141 cm ²
	Mass	191 kg
Main Windings	Current Density	7.6 A/mm ²
	Volt/turn	5 V

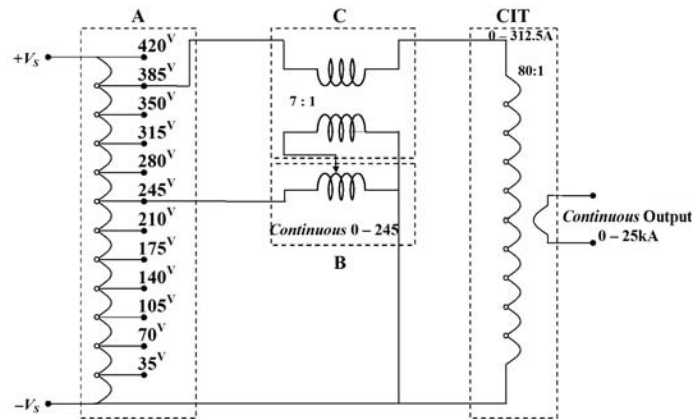


Figure 6. The circuit diagram of the CIS and its control system

Fig. 7 shows the schematic feature of the CIS incorporating the microprocessor controlled tapchanger system. Moreover, the CIS system, which is controlled by the FPGA chip, the main processor unit, is virtually protected against EMI by being confined within a two layer (4 mm thickness) iron sheet box.

It stands to reason that, due to shielding effect deficiency, there is a likelihood of false data being transmitted to the control box by the

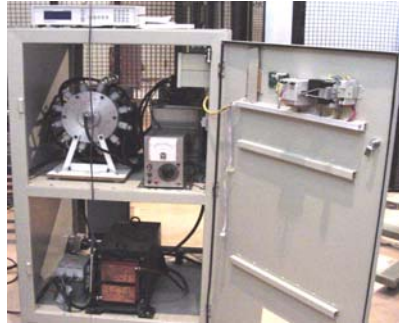


Figure 7. The prototype 25 KA CIS incorporating the microprocessor controlled tap-changer system.

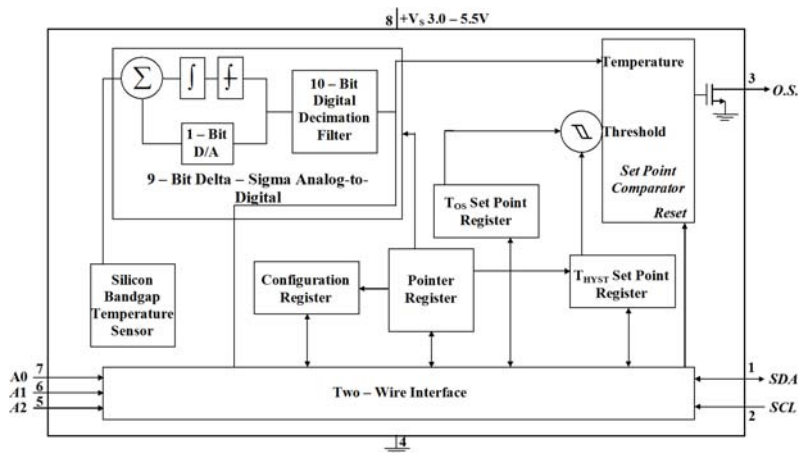


Figure 8. Simplified block diagram of LM75.

temperature sensor data. The unpredictable transient state is even more of a concern than the performance of wire shielding because this may cause data disorder in the temperature readings as well as erratic overload relay. The type of the temperature sensor used in the CIS is the LM75 which is a Delta-Sigma analog-to-digital converter with a simplified block diagram shown in Fig. 8. The host can query the LM75 at any time to read temperature. The open-drain over-temperature shutdown (OS) output becomes active when the temperature exceeds a preprogrammed limit. This pin can operate in either comparator or “interrupt” mode.

The host can program both the temperature alarm threshold

(T_{OS}) and temperature at which the alarm condition stops (T_{HYST}). In addition, the host can read back the contents of the LM75's T_{OS} and T_{HYST} registers. Three pins (A0, A1, and A2) are available for address selection. The LM75's 3.0 V to 5.5 V supply voltage range, low supply current, and I²C interface make it ideal for a wide range of applications such as CIS. Thus, the FPGA device must be located next to the LM75 temperature sensor, for the encoding software. It must be placed in a metal box according to the required shielding effectiveness in the CIS as mentioned in the previous section (two layer iron shield with 2 mm thickness).

There are eight LM75 devices to monitor eight 0–200°C temperatures in the CIS enclosure. The channel capacity is considered at 9600 bits/sec after mux/demux is performed with 400 bits/sec sensor output and is repeated each block three times. As it is possible to use eight sensors via I²C protocol, the 3200 bits/sec is transmitted through channel three times.

4.2. Application and Implementation of Convolutional Codes in CIT Systems

4.2.1. A Preliminary Discussion on Convolutional Codes

Generally, the probability of error can be reduced by transmitting more bits as parity checks than needed to represent the information being sent, and convolving each bit with neighboring bits so that if one transmitted bit got corrupted, enough information is carried by the neighboring bits to estimate what the corrupted bit was [5, 6, 8]. This approach of transforming a number of information bits into a larger number of transmitted bits is called channel coding, and the particular approach of convolving the bits to distribute the information is referred to as convolution coding [17]. The ratio of information bits to transmitted bits is the code rate (less than 1) and the number

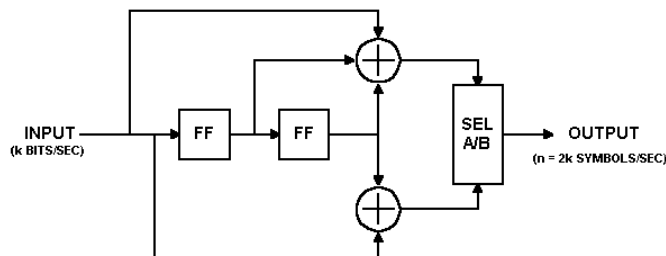


Figure 9. A convolution encoder.

of information bits over which the convolution takes place is the constraint length [5, 6]. Fig. 9 shows the typical convolution encoder. This is a convolution encoder of code rate $1/2$. This means that there are two output bits for each input bit. Here the output bits are transmitted one after another, two per clock cycle. The outputs z_1 and z_2 are defined as:

$$\begin{aligned} z_1 &= x(n) \oplus x(n-1) \oplus x(n-2) \\ z_2 &= x(n) \oplus x(n-2) \end{aligned}$$

where $x(n)$ is the present input bit, $x(n-1)$ is the previous bit, etc.

The input connections to the XORs can be written as binary vectors [1 1 1] and [1 0 1] which are known as the generating vectors or generating polynomials for the code.

According to the system characteristics, the 6400 bits/sec (i.e., 3200 bits of data and 3200 bits of parity checks) is transmitted through the channel with code rate $1/2$. Hence, this transmission rate is lower than the channel capacity which fulfills Shannon capacity criterions.

4.2.2. Simulation Results

The designed simulation source code comprises a test driver routine and several functions. This code simulates a link through an Additive White Gaussian Noise (AWGN) channel estimated as noise in the CIT system noise from source data to destination with a Viterbi decoder [17].

The test driver first dynamically allocates several arrays to store the source data, the convolutionally encoded source data, the output of the AWGN channel, and the data output by the Viterbi decoder. Next, it calls the data generator, convolution encoder, channel simulator, and Viterbi decoder functions in turn. It then compares the source data output by the data generator to the data output by the Viterbi decoder and counts the number of errors.

The simulation results for several code rates are shown in Fig. 10. Due to no limitation of channel capacity, the use of code rate $1/2$ provides good performance for error correction in the CIT system.

4.2.3. Methodology Evaluations

It is important to run controlled experiments to compare the relative effectiveness of the measurement results with the simulation results for the evaluation of the secondary shielding performance. Thus, an external transient high magnetic field generated by a high voltage pulse transformer [18] was applied to the CIS thereby creating artificially

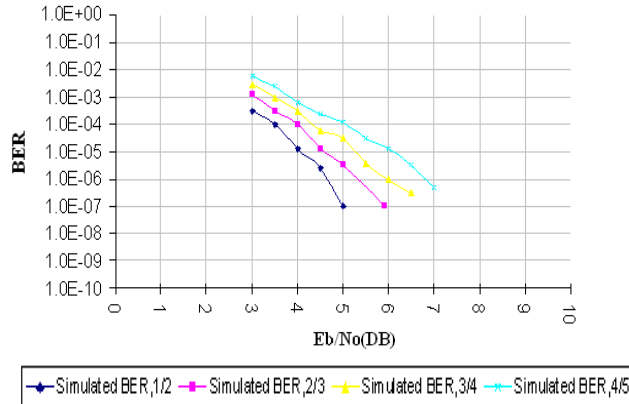


Figure 10. Simulation results for BER performance for several code rates.

undesired conditions. The pulse transformer was set to provide for the undesired condition where the conventional shielding is deficient and disturbed signaling may occur. This phenomenon was verified by an incorrect reading on the temperature indicator being compared with the true temperature reading. Furthermore, the proposed secondary shielding was added to the control system software and the experiment was repeated. The error correction system with the code rate of 1/2 was used.

The test was performed by injecting noise to the system several times. False temperature readings were not observed. However, for the verification of the simulation results, the test was repeated up to 1000 times. For statistical purpose, the test was done for 20 cycles. The results prove that the probability of BER occurrence for the temperature data signaling in the CIS is within the range of 0.0001 to 0.001.

4.2.4. New Approach of EMC Study in the CIS Enclosure

This paper proposes the algorithm shown in Fig. 11, based on a five step design for shielding purposes considering EMC procedures for the CIS. The steps are:

- a) Magnetic field simulation,
- b) Optimized position of sensitive elements (such as control wires) in the CIS enclosure considering interference fields,
- c) Shielding of control box,

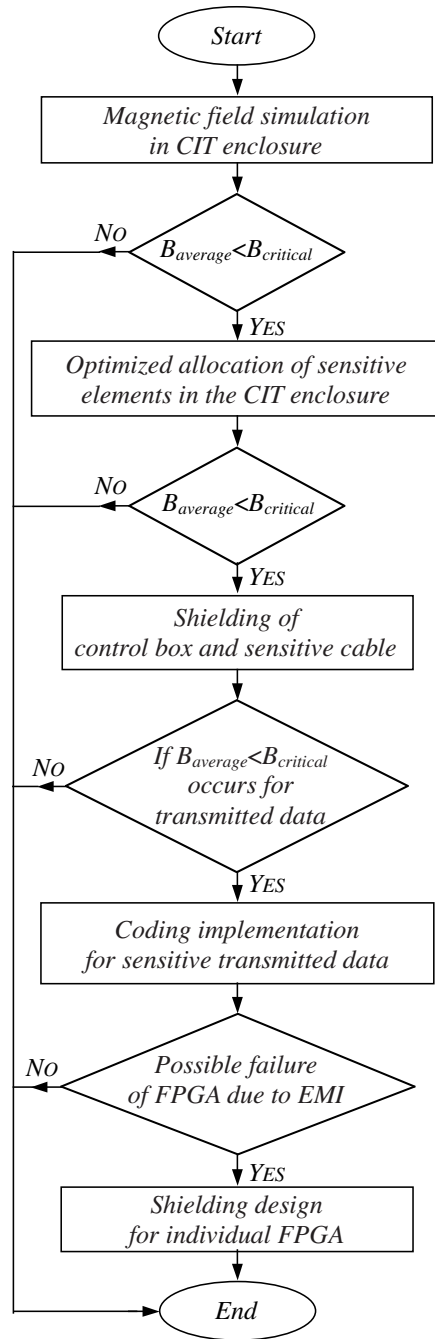


Figure 11. Algorithm of the proposed approach.

- d) Coding implementation for sensitive transmitted data, and
- e) Shielding design for the FPGA locating close to the measuring sensors for the case 4 purpose.

To better understand the contribution of the proposed algorithm, the designed steps are briefly explained. The simulation of the magnetic field is performed by using a dipole acting as the field source. This approximate model can show the EMI occurrence in the system. High EMI values make the wiring route optimization of the sensitive elements necessary. Thus, one major challenge is to ensure the transients be neutralized by EMC issues and wiring routes. The optimal route is selected, based upon various criteria such as monetary cost minimization, voltage drop, and quality (EMC) parameters. Based upon the aforementioned criteria, by using analytical hierarchy process (AHP), the intelligent choice of optimal cabling routes can be achieved [16].

When the redesign of sensitive element allocation is not sufficient, the shielding of sensitive elements, specifically control boxes, must be done (Section 3.1). However, the occurrence of undesired interferences in special conditions causing inaccurate performance of the control circuits or transmission signals passing through the wires is a statistical matter. Thus, the use of convolutional codes regarding the system specification is suitable. Hence, the FPGA devices for the encoding software which are close to the individual measuring sensors must be shielded based on the discussion given in Section 4.1.

5. CONCLUSION

As an electrical utility you have the right to demand that every piece of power equipment installed on your system meets your exact specifications. The high current of the CIS produces large fields that interfere with transmitted signals. Thus, its compatibility with the internal and external propagation and low-frequency and high-frequency disturbances within electromagnetic environment must be ensured.

The simulation and experimental results revealed that iron can act as an optimal electromagnetic shielding material against EMI. In this regard, a 6 mm body thickness for a 25 kA current injection system as a case study was tested and good shielding efficiency of 68 dB was achieved. From a nonstructural point of view, higher efficiency occurs when two layer shielding is used. Considering the distance between the layers as a second effective parameter, a two layer shielding combination of iron with 6 mm thickness was the final approach for higher efficiency. Extraordinary conditions may cause

detrimental effects on the transmitted signals. Thus, an algorithm based on convolution codes is proposed in the body of the control system as a secondary EMC protection. As the data of temperature sensor are very sensitive to the EMI, a set of encoder and decoder for implementation of convolution codes are proposed. It will create more error-free outputs. Thus, the FPGA located close to each temperature sensor must be shielded in an appropriate manner. According to the simulation source code, the use of a code rate $1/2$ provides good performance for error correction in the CIS. This was also confirmed by the methodology evaluation.

Hence, when considering EMC as a general approach, the proper coding can be used as secondary shielding. It provides more reliability for the error-free operation of the system.

REFERENCES

1. Heydari, H. and F. Faghihi, "Hybrid winding configuration in high current injection transformers based on EMC issues," *IET Electric Power Applications*, Accepted and to be published, 2008.
2. Sandrolini, L., A. Massarini, and U. Reggiani, "Transform method for calculating low-frequency shielding effectiveness of planar linear multi layered shields," *IEEE Transaction on Magnetics*, Vol. 36, 3910–3919, Nov. 2000.
3. Molyneux-child, J. W., "EMC shielding materials," TD, BSc (Eng), MCIM, Group Chairman, Surrey Group, Newnes, 1997.
4. Celozzi, S., "New figures of the characterization of the performance of shielding enclosures," *IEEE Transactions, Electromagnetic Compatibility*, Vol. 46, No. 1, 142–146, Feb. 2004.
5. dos Santos, M. P. F., W. A. Clarke, H. C. Ferreira, and T. G. Swart, "Correction of insertions/deletions using standard convolutional codes and the Viterbi decoding algorithm," *IEEE Information Theory Workshop*, 187–190, Paris, France, Apr. 2003.
6. Swart, T. G. and H. C. Ferreira, "Insertion/deletion correcting coding schemes based on convolution coding," *Electronics Letters*, Vol. 38, No. 16, 871–873, Aug. 2002.
7. Berrou, C., A. Glavieux, and P. Thitimajshima, "Near shannon limit error-correcting coding and decoding: Turbo-codes," *Proceedings of ICC*, 1993.
8. Brink, B., H. C. Ferreira, and W. A. Clarke, "Pruned convolutional codes for flexible unequal error protection against insertion/deletion/reversal errors," *Proceeding ISIT2000*, Sorrento, Italy, Jun. 2000.

9. Tai, C.-C. and Y.-L. Pan, "Finite element method simulation of photo inductive imaging for cracks," *Progress In Electromagnetics Research Letters*, Vol. 2, 53–61, 2008.
10. Vaish, A. and H. Parthasarathy, "Analysis of a rectangular waveguide using finite element method," *Progress In Electromagnetics Research C*, Vol. 2, 117–125, 2008.
11. Zhou, X. and G. W. Pan, "Application of physical spline finite element method (PSFEM) to fullwave analysis of waveguides," *Progress In Electromagnetics Research*, PIER 60, 19–41, 2006.
12. Roy, A., S. Ghosh, and A. Chakrabarty "Simple crosstalk model of three wires to predict nearend and farend crosstalk in an EMI/EMC environment to facilitate EMI/EMC modeling," *Progress In Electromagnetics Research B*, Vol. 8, 43–58, 2008.
13. Lindell, V. and A. H. Sihvola, "Reflection and transmission of waves at the interface of perfect electromagnetic conductor (PEMC)," *Progress In Electromagnetics Research B*, Vol. 5, 169–183, 2008.
14. Sharaa, D. N. Aloï, and H. P. Gerl, "EMC model-based test-setup of an electrical system," *Progress in Electromagnetics Research B*, Vol. 11, 133–154, 2009.
15. Faghihi, F., "Design optimization of current injection transformer based on EMC considerations," PhD Thesis, Iran University of Science and Technology, Iran, July 2008.
16. Heydari, H., F. Faghihi, R. Sharifi, and A. M. Poursoltanmohammadi, "Superconducting technology for over-current limiting in a 25 KA current injection system," *IOP Journals, Superconductor Science and Technology*, Vol. 21, 2008.
17. Mori, T. and H. Imai, "Viterbi decoding considering insertion/deletion errors," *Proc. ISIT1995*, 145, Whistler, B.C., Canada, Sept. 1995.
18. Vahedi, A., H. Heydari, and F. Faghihi, "Analysis and simulation of pulse transformer considering leakage inductance and capacitance," *IEE Conference, CIRED 2005*.